



OPEN ACCESS

EDITED BY

Li Li,
Northwest A&F University, China

REVIEWED BY

Yuan Jia,
North China University of Science and
Technology, China
Anming She,
Tongji University, China

*CORRESPONDENCE

Yang Ding,
✉ ceyangding@zju.edu.cn

RECEIVED 19 August 2023

ACCEPTED 27 September 2023

PUBLISHED 17 October 2023

CITATION

Dong J, Li L, Shi Z, Ding Y, Chen X and
Zong Y (2023), Strength development and
hydration products of alkali-activated
Pisha sandstone geopolymer cement.
Front. Mater. 10:1280088.
doi: 10.3389/fmats.2023.1280088

COPYRIGHT

© 2023 Dong, Li, Shi, Ding, Chen and
Zong. This is an open-access article
distributed under the terms of the
[Creative Commons Attribution License
\(CC BY\)](https://creativecommons.org/licenses/by/4.0/). The use, distribution or
reproduction in other forums is
permitted, provided the original author(s)
and the copyright owner(s) are credited
and that the original publication in this
journal is cited, in accordance with
accepted academic practice. No use,
distribution or reproduction is permitted
which does not comply with these terms.

Strength development and hydration products of alkali-activated Pisha sandstone geopolymer cement

Jingliang Dong¹, Lianghua Li¹, Zhenhua Shi¹, Yang Ding^{2*},
Xiaolei Chen¹ and Yingliang Zong¹

¹School of Civil Engineering and Architecture, East China Jiaotong University, Nanchang, China,

²Department of Civil Engineering, Hangzhou City University, Hangzhou, China

Pisha sandstone (PS) is a unique geological structure in the Yellow River basin in China and is a general term for a rock interlayer composed of sandstone, sand shale, and muddy sandstone. The collapsibility of PS results in a high erosion rate and poor vegetation due to its low diagenetic potential and weak structural strength. This study showed that PS can be converted into geopolymer cement by mixing with a suitable alkali activator. PS was converted to geopolymer cement for construction to control soil erosion and conserve the soil and water in this area. Slag was used as a mineral additive to improve the performance of alkali-active PS geopolymer cement in this study. The influence of slag replacement level, NaOH dosages, and curing age on the compressive strength of alkali-activated PS was investigated. Scanning electron microscopy (SEM)/energy dispersive X-ray (EDS), thermogravimetric analyses (TG/DTG), and X-ray diffraction (XRD) were used to analyze the hydration products and microstructure of alkali-activated PS. The results showed that when the samples had 40 wt.% slag, 1.5 wt.% NaOH, and 4.0 wt.% Na₂SiO₃, their compressive strength could reach 82.0 MPa at 90 days. Compared with the samples with activator and without activator, the compressive strength increased by 6,664% and 9,011%, respectively. The hydration products were C-S-H gel, geopolymer gel, and calcium carbonate crystals. With 10 wt.% slag as a mineral additive, 1.5 wt.% NaOH, and 4 wt.% Na₂SiO₃ as an activator, the carbonation ratio of C-S-H gel was 49.3%.

KEYWORDS

Pisha sandstone, alkali-activated, slag, mechanical properties, microstructures, thermal analysis

1 Introduction

Pisha sandstone (PS) is a kind of interbedded mudstone and sediment rock composed of Paleozoic Permian, Mesozoic Triassic, Jurassic, and Cretaceous thick sandstone. It is widely distributed in the border area of the Shanxi, Shaanxi, and Mongolia provinces in the middle reaches of the Yellow River in China (Zhang et al., 2022). PS is seriously weathered after environmental erosion, which produces a large amount of sand and weathering in the Yellow River. It is the center of severe erosion in the middle reaches of the Yellow River, and the soil erosion module is (3~4) 10⁴ t/(km²·a) (Wang et al., 2022). Liu et al. (2023) suggested that the weathered clay minerals of PS are mainly composed of fine soil such as montmorillonite,

which has good mechanical properties in the natural state. Gao et al. (2021) reported soil erosion was caused by the interaction of wind erosion, hydraulic erosion, and gravity erosion as it has low diagenetic potential and structural strength. However, the clay material between the particle pores will absorb water, resulting in the loss of the particles, showing the characteristics of breaking into sand in water and being easily weathered. Wei et al. (2020) reported that the main effect of hydraulic erosion on PS was weakening the cohesion within the rock mass and increasing its porosity.

Previous studies have mainly focused on exploring the natural structure of PS and the causes of its collapse into sand after encountering water (Wei et al., 2020; Gao et al., 2021; Liu et al., 2023). However, the literature focusing on improving the performance of PS is scarce. To reduce soil erosion, converting PS into geopolymer cement and utilizing PS resources is a very effective method.

The production of geopolymer has lower energy consumption, lower CO₂ emissions, and higher chemical resistance and has more economic benefits than traditional Portland concrete (Yang et al., 2021; Han et al., 2023). Previous studies have shown that geopolymer is composed of silicon-oxygen tetrahedral (SiO₄)⁴⁻ and aluminum-oxygen tetrahedral (AlO₄)⁵⁻. It has different structures and properties due to different silicon-aluminum ratios. When the ratio of silicon-aluminum reaches 2:1, the tetrahedral arrangement structure is the most reasonable and the best mechanical properties are achieved (Luo et al., 2023; Pratap et al., 2023). Some references showed that the commonly used raw materials of geopolymer cement are fly ash, metakaolin, coal gangue, and other high silicon aluminum and low calcium industrial wastes. This is because the performance of the polymer depends on the dissolution amount of Si, Al, and other elements in the raw material. The higher the dissolution amount of Si, Al, and other elements, the more (SiO₄)⁴⁻ and (AlO₄)⁵⁻ three-dimensional mesh gels and the better the mechanical properties of the polymer (Abdellatif et al., 2023; Alaneme et al., 2023; Yi et al., 2023).

The natural PS shows different colors due to the different chemical compositions in northwest China (Liu et al., 2023). However, PS of different colors contain a lot of silica and alumina, and the molar ratio of Al₂O₃/SiO₂ is between 1/3.5 and 1/5.8. Therefore, PS may have the potential to serve as a source of aluminosilicate. However, not all silica and alumina are involved in the synthesis reaction (Dhakal et al., 2022). From the results of this study, the rate of the dissolution of Al and Si from natural PS is insufficient to produce a geopolymer with the desired properties. Factors such as increasing the molar Si-Al ratio and CaO dosage have positive effects on the properties (compressive strength, microstructures, and hydration products) of geopolymer cement (Dhakal et al., 2022; Feng and Liu, 2022). The slag used in this research contains a high content of active silica, active alumina, and calcium oxide. Therefore, it may be a relatively desirable aluminosilicate when it is added to PS to synthesize geopolymer. Previous literature revealed that a desired geopolymer gel will be formed in a shorter setting time (Wu et al., 2021) when slag is combined with an optimum amount of alkali-activator.

This study showed deficiencies in the active SiO₂ and active Al₂O₃ in the natural PS. By adding mineral additives such as slag to provide active SiO₂ and active Al₂O₃, PS can be used as geopolymer cement. The effects of different NaOH dosages, slag dosages, and ages on compressive strength were observed. The hydration products and microstructures of the samples with different NaOH and slag dosages were analyzed by XRD, SEM, and EDS.

TABLE 1 Chemical compositions of PS and slag (wt.%).

| Material | LOI | SiO ₂ | Al ₂ O ₃ | Fe ₂ O ₃ | CaO | MgO | K ₂ O |
|----------|------|------------------|--------------------------------|--------------------------------|-------|------|------------------|
| Red PS | 1.03 | 65.63 | 14.26 | 9.28 | 3.49 | 5.12 | 0.89 |
| White PS | 1.34 | 62.95 | 14.36 | 4.03 | 8.02 | 4.94 | 0.76 |
| Slag | 1.89 | 30.32 | 9.69 | 0.63 | 44.46 | 9.34 | 0.69 |

2 Experiment

2.1 Raw materials

The main raw materials used in this study are white natural PS and red natural PS from Inner Mongolia, northwest China. S95 grade slag from Rong Changsheng Co., Ltd., was selected as the mineral additive. The measured specific gravity and specific surface area of slag were 2.9 and 4,300 cm²/g, respectively. The PS was calcined for 2 h at 750°C and then grounded to 80 μm before tests. The natural PS and slag were analyzed by X-ray fluorescence (XRF) and X-ray diffraction (XRD) at the State Key Laboratory of East China, Jiaotong University, Nanchang, China. The results of the XRD and XRF tests are shown in Table 1 and Figure 1.

The main activator used in this study was NaOH (analytically pure, content > 99 wt.%). Sodium silicate solution (water glass) provided by China Henan Hengyuan New Material Co., Ltd., was used as an auxiliary activator. The chemical composition of the water glass was: 7.5 wt.% of sodium oxide (Na₂O), 23.5 wt.% of silicon oxide, and 69 wt.% of water; pH = 11.

2.2 Sample preparation and methods

All test specimens were classified into two groups. Group 1 (Table 2) was used to investigate which color of PS has better potential as a source of aluminosilicate. The white (Figure 2B) and red (Figure 2A) PSs were activated with or without different activators and then tested for compressive strength at different ages.

In group 2 (Table 3), slag was added to the paste as the mineral additive. The effects of different slag dosages (0, 10 wt.%, 20 wt.%, 30 wt.%, and 40 wt.%), different contents of NaOH [0.5 wt.%, 1.0 wt.%, 1.5 wt.%, 0.5 wt.% NaOH indicates a molarity of NaOH of 1.5 mol/L. A 1.0 wt.% of NaOH (1.0 wt.%) indicates a 3 mol/L molarity of NaOH. A 1.5 wt.% of NaOH indicates a molar concentration of NaOH of 4.5 mol/L.], and different curing ages (1d, 3d, 7d, 28d, 90d) on the compressive strength of alkali-activated white PS were investigated.

After mixing different dosages of slag with PS, water and activator were added to the mixtures for the samples of alkali activation. The pastes were stirred with an N-50-1425 rpm blender. Steel cylindrical molds (Φ50 mm × 130 mm) were used to transfer the resulting pastes. The cylindrical samples were formed by pressure (50 kN), with a size of Φ50 mm × 50 mm. After removal from the mold, 15 samples of each formulation were covered with a plastic bag (preventing evaporation) and cured in an 80°C (Fu et al., 2021; Luo et al., 2022; Snellings et al., 2022; Wu et al., 2022) air box for 12 h. The samples were then set at room temperature and further solidified and hardened at 20°C for 1, 3, 7, 28, and 90 days. In the last step, the compressive strength of the three samples of each formulation was measured at 1, 3, 7, 28, and 90 days.

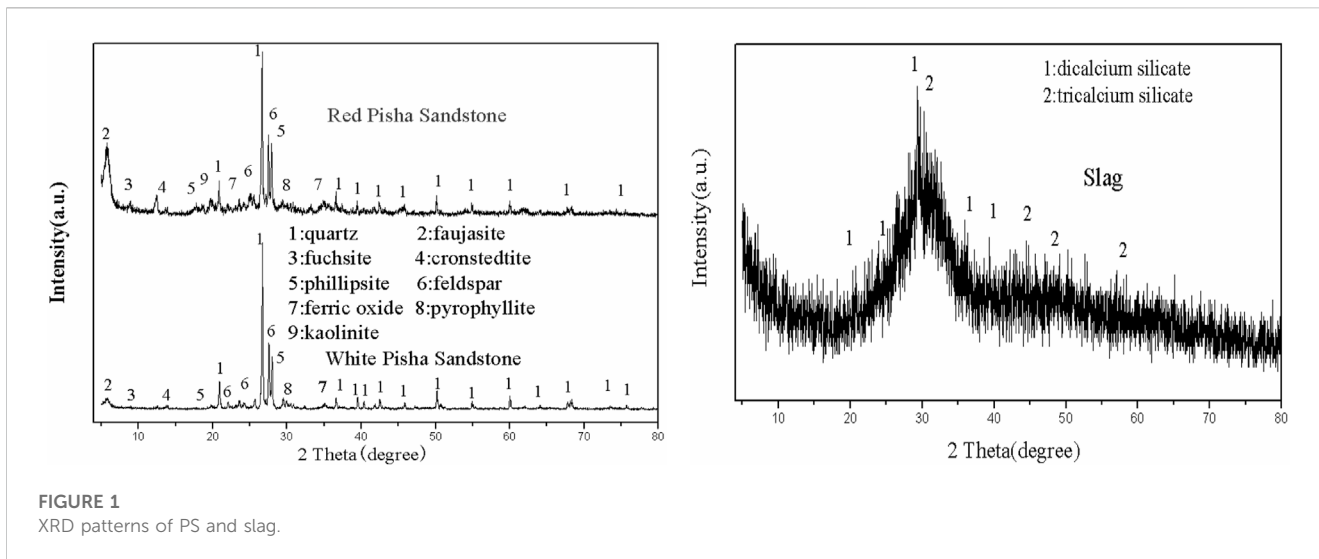
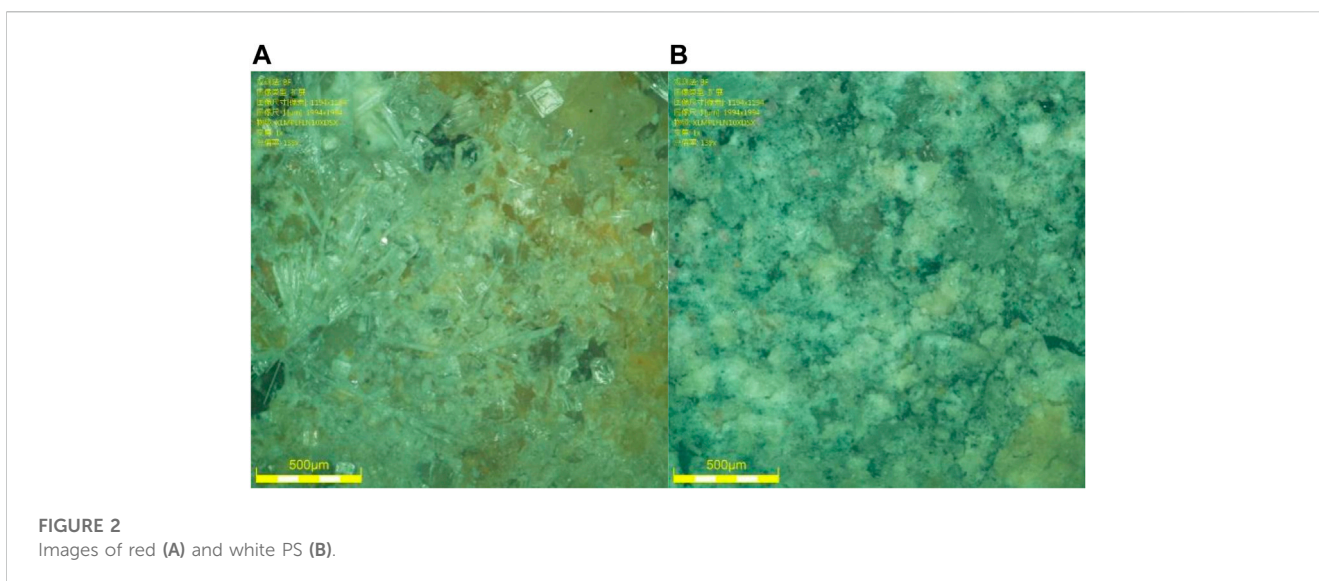


TABLE 2 Mix proportions and test results for group 1 specimens.

| Type | Mix proportions (g) | | | | | Compressive strength (MPa) (white/red) | | | | |
|------|---------------------|----------------------------------|------|-------|-------|--|----------|----------|----------|----------|
| | Slag | Na ₂ SiO ₃ | NaOH | PS | Water | Curing ages [day(s)] | | | | |
| | | | | | | 1 | 3 | 7 | 28 | 90 |
| A0 | 0 | 0 | 0 | 206.2 | 16.5 | 0.3/0.4 | 0.4/0.5 | 0.4/0.6 | 0.8/1.1 | 0.9/1.2 |
| A1 | 0 | 8.2 | 1.03 | 196.8 | 16.5 | 5.7/5.2 | 5.8/5.5 | 5.8/5.6 | 5.9/5.7 | 6.2/5.8 |
| A2 | 0 | 8.2 | 2.06 | 195.7 | 16.5 | 6.5/6.2 | 7.0/6.6 | 7.6/7.3 | 7.6/7.2 | 7.8/7.3 |
| A3 | 0 | 8.2 | 3.09 | 194.7 | 16.5 | 10.1/9.2 | 10.5/9.2 | 10.5/9.3 | 10.6/9.4 | 10.7/9.5 |

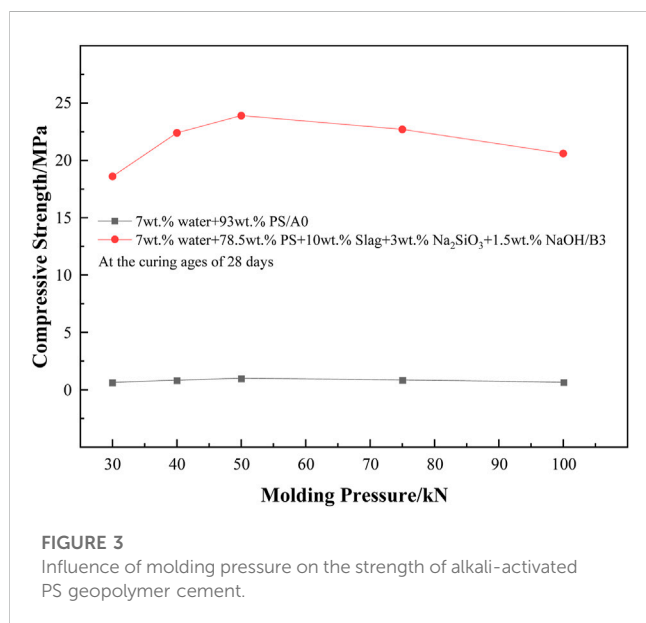


The hydration products and microstructures of alkali-activated PS geopolymer cement samples (group 2) were analyzed by X-ray diffraction (XRD, a Siemens D500 diffractometer [copper radiation after nickel filtration], acquisition range of 4°–80°(2θ); the scan rate

was 2°/min and the step size was 0.02) and energy-dispersive X-ray (EDS, a JEOL JSM 6460 Scanning Electron Microscope at an accelerating voltage of 20 kV) combined with scanning electron microscopy (SEM, a JEOL JSM 6460 Scanning Electron Microscope

TABLE 3 Mix proportions and test results for alkali-activated white PS geopolymer cement.

| Type | Mix proportions (g) | | | | | Compressive strength (MPa) | | | | |
|------|---------------------|----------------------------------|------|-------|-------|----------------------------|------|------|------|------|
| | Slag | Na ₂ SiO ₃ | NaOH | PS | Water | Curing ages [day(s)] | | | | |
| | | | | | | 1 | 3 | 7 | 28 | 90 |
| B1 | 20.6 | 8.2 | 1.0 | 176.2 | 16.5 | 15.4 | 15.2 | 15.6 | 16.6 | 16.7 |
| B2 | 20.6 | 8.2 | 2.1 | 175.2 | 16.5 | 18.2 | 18.2 | 19.0 | 19.2 | 19.2 |
| B3 | 20.6 | 8.2 | 3.1 | 174.2 | 16.5 | 21.2 | 21.4 | 21.5 | 22.2 | 22.5 |
| C1 | 41.2 | 8.2 | 1.0 | 155.6 | 16.5 | 24.2 | 24.2 | 25.3 | 25.3 | 25.7 |
| C2 | 41.2 | 8.2 | 2.1 | 154.8 | 16.5 | 29.0 | 29.8 | 30.6 | 30.9 | 30.8 |
| C3 | 41.2 | 8.2 | 3.1 | 153.8 | 16.5 | 35.5 | 35.6 | 35.8 | 35.8 | 36.3 |
| D1 | 61.8 | 8.2 | 1.0 | 134.2 | 16.5 | 38.0 | 38.4 | 39.0 | 39.6 | 39.7 |
| D2 | 61.8 | 8.2 | 2.1 | 133.2 | 16.5 | 46.3 | 47.0 | 47.5 | 47.6 | 48.2 |
| D3 | 61.8 | 8.2 | 3.1 | 132.2 | 16.5 | 57.0 | 57.3 | 57.9 | 57.8 | 58.7 |
| E1 | 82.4 | 8.2 | 1.0 | 113.6 | 16.5 | 61.7 | 62.0 | 62.5 | 62.8 | 63.0 |
| E2 | 82.4 | 8.2 | 2.1 | 112.6 | 16.5 | 68.5 | 69.0 | 69.2 | 69.5 | 69.8 |
| E3 | 82.4 | 8.2 | 3.1 | 111.6 | 16.5 | 80.5 | 81.7 | 81.8 | 81.9 | 82.0 |



at an accelerating voltage of 20 kV) at the State Key Laboratory of East China Jiaotong University, Nanchang, China.

Figure 3 shows the effect of molding pressure on the strength of alkali-activated PS geopolymer cement. As the molding pressure increased from 30 to 50 kN, the compressive strength of A0 increased from 0.65 to 1 MPa. However, when the molding pressure increased from 50 to 100 kN, the compressive strength of A0 did not change significantly. This indicated that the change of molding pressure did not significantly affect the compressive strength of A0, and the optimal molding pressure was approximately 50 kN. For B3, as the molding pressure increased from 30 to 50 kN, the

compressive strength of B3 increased from 18.6 to 23.9 MPa. However, as the molding pressure increased from 50 to 100 kN, the compressive strength of B3 decreased from 23.9 to 20.6 MPa. The results showed that the alkali-activated PS geopolymer cement (PS) had the highest compressive strength when the molding pressure was approximately 50 kN. When the molding pressure was greater than or less than 50 kN, the compressive strength was reduced. Superfluous molding pressure resulted in NaOH being squeezed out of the PS paste, which led to insufficient amounts of water and NaOH for alkali excitation. Inadequate molding pressure resulted in the presence of numerous pores in the PS matrix, which prominently reduced the compressive strength of PS.

3 Results and discussion

3.1 The compressive strength of alkali-activated PS geopolymer cement without slag

The compressive strengths (Table 2; Figure 4A) of white and red PSs that were not alkali-activated were relatively low (approximately 1 MPa at 90 days). However, the compressive strengths of white and red PSs with 0.5 wt.% NaOH and 4 wt.% Na₂SiO₃ (Figures 4B, C) as activators increased from 5.7 and 5.2 MPa at day 1 to 6.2 and 5.8 MPa at 90 days, respectively. The compressive strength of PS after being alkali-activated increased significantly. The addition of NaOH significantly affects the compressive strength of alkali-activated white and red PSs. With the NaOH dosages increasing from 0.5 wt.% to 1.5 wt.%, the compressive strength of alkali-activated white and red PSs increased from 6.2 and 5.8 MPa to 10.7 and 9.5 MPa, respectively, at 90 days. However, curing ages have less influence on the compressive strength of alkali-activated PS than the NaOH dosage.

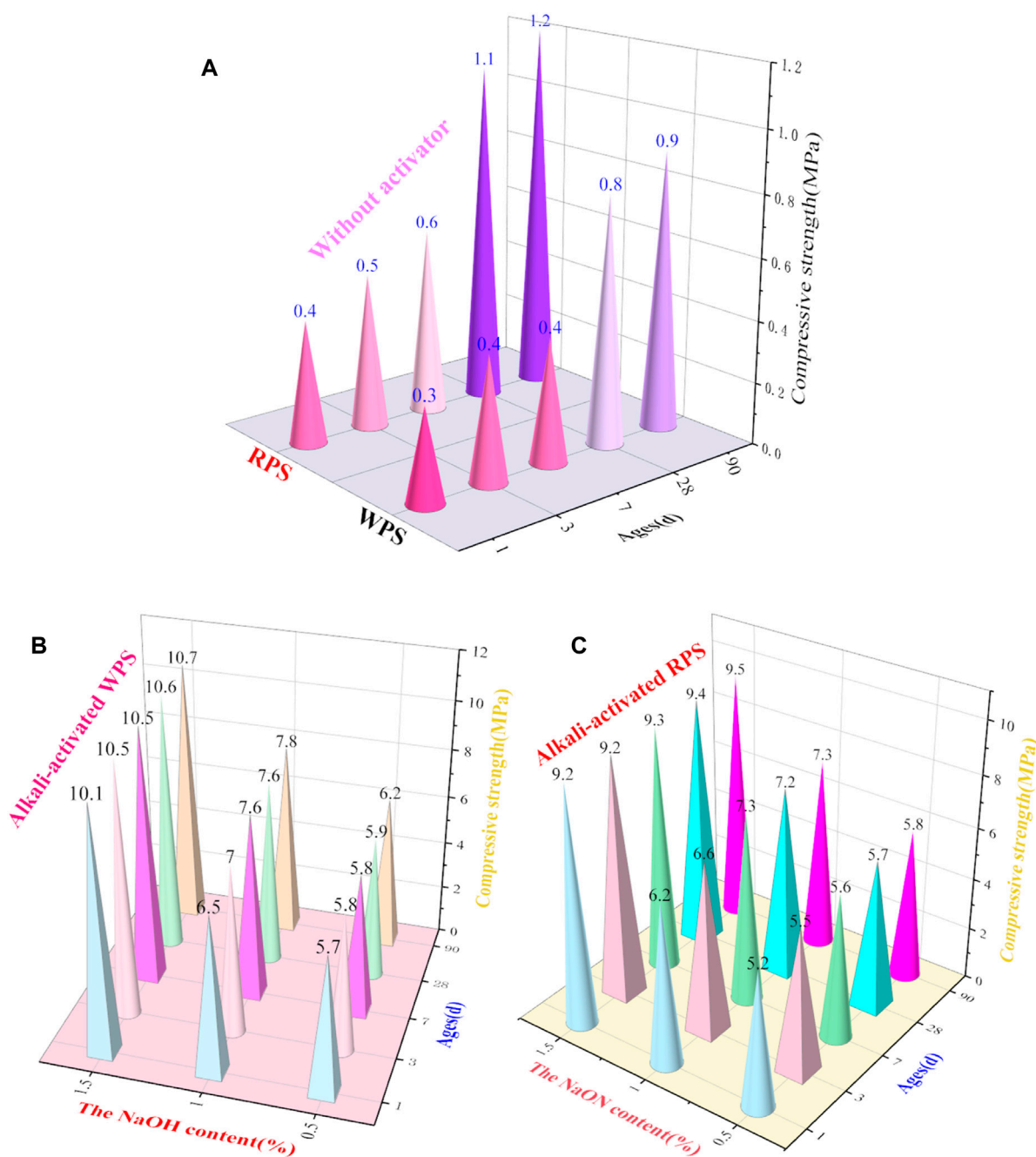


FIGURE 4 Compressive strength of the red (C) and white (B) PSs with or without different contents (A) of NaOH and 4% Na₂SiO₃ as an activator at different ages.

The compressive strength of red PS was slightly higher than that of white PS. This was caused by the fact that although white and red PSs have similar chemical compositions (shown in Table 1 and Figure 1), the red PS has more clay. Figure 4 shows that the strength development of alkali-activated PS almost finished after 7 days. This was because of the faster hydration rate of the alkali-activated geopolymer cement (Zhong et al., 2023). The compressive strength of PS with an activator was greatly improved compared with the PS. Additionally, the compressive strength of alkali-activated white PS with 1.5 wt.% NaOH at day 7 increased by 2,525% compared with that of white PS. The compressive strength of

alkali-activated red PS with 1.5 wt.% NaOH at day 7 increased by 1,450% compared with that of red PS. This occurred because of the polymerized Al and Si network that was obtained from the reaction between active silica and alumina in the PS paste when activated by NaOH and Na₂SiO₃ (Feng and Li, 2023). There is an optimum addition for the activator although it does depend on the different colors of the PS. The compressive strength of PS increased with the increase in the NaOH dosage. As shown in Figure 4, with the same activator, the compressive strength of alkali-activated white PS was higher than that of the red PS. This difference is due to the fact that white PS contains more CaO as the calcium content,

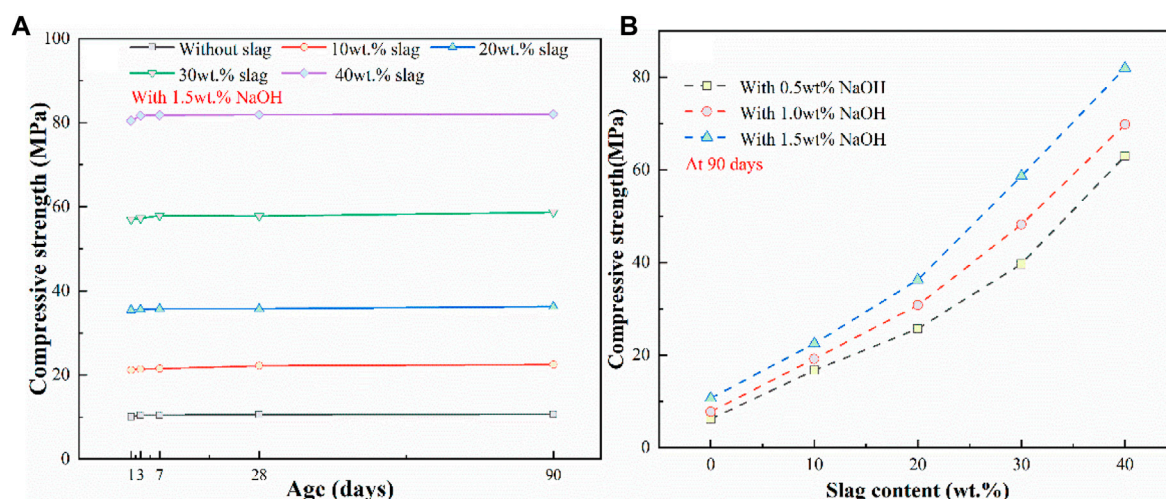


FIGURE 5 Effect of slag dosage, age (A), and different NaOH dosages (B) on compressive strength.

which can improve the properties of the geopolymer (Yi et al., 2023). Ages have a slight effect on the compressive strength of alkali-activated PS. Additionally, it can be observed that the white PS has better potential than the red PS.

However, alkali-activated PS without slag still showed a low compressive strength and weak structure for engineering. Thus, slag was added to alkali-activated PS geopolymer cement to improve the compressive strength and microstructure.

3.2 Effect of slag dosages and ages on the compressive strength of alkali-activated white PS geopolymer cement

Figures 5A, B shows the effects of slag content, ages, and NaOH content on the mechanical property of alkali-activated white PS geopolymer cement. Compared with the slight effect of age on mechanical property, the NaOH dosages significantly affect the compressive strength of alkali-activated white PS geopolymer cement.

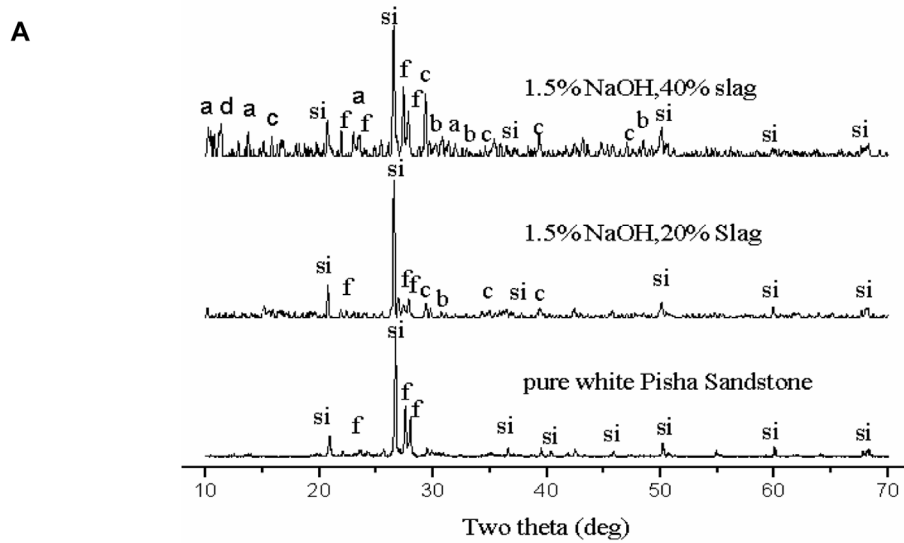
At the curing age of 90 days, the compressive strength of alkali-activated white PS geopolymer material added with 1.5 wt.% NaOH increased from 10.7 to 82.0 MPa as the slag dosage ranged from 0 to 40 wt.%. The compressive strength of alkali-activated white PS greatly increased with the increase in slag dosage. This can be attributed to the addition of a certain amount of slag, which will sufficiently polymerize the Al and Si network, thus compensating for the deficiencies in available SiO₂, Al₂O₃, and CaO in white PS. The present study demonstrated that the addition of slag provides active aluminum and silicon to intensify the three-dimensional amorphous and/or semi-crystalline polymer structures. Additionally, alkali metal cations will compensate for the negative charges, which are caused by Al substitution (Lv et al., 2021). Furthermore, Figure 5A shows that the compressive property of alkali-activated white PS with dissimilar slag contents slightly increased with the increase in age. The Al and Si network polymerization reaction generated by the reaction of activated silica and alumina was completed within 24 h.

As was shown in Figure 5B, the compressive strength of alkali-activated PS geopolymer cement added with diverse slag contents was significantly fortified as NaOH content ranged from 0.5 to 1.5 wt.%. At the age of 90 days, the mechanical property of alkali-activated PS geopolymer material with 40 wt.% slag increased from 63 to 80 MPa as NaOH content ranged from 0.5 to 1.5 wt.%. The content of sodium hydroxide had a more significant influence on the compressive strength as the slag dosage increased. There is an optimum addition of NaOH as the main activator, which is independent of slag dosage. The most suitable addition of NaOH is 1.5 wt.% in alkali-activated PS geopolymer material. Excessive NaOH content can increase the cost of alkali-activated PS geopolymer cement. According to previous results (Liu et al., 2023), the optimum dosage of the activator lies on the precursor, which must be sufficient to meditate the charges of the Al and Si tetrahedral. Excessive NaOH or Na₂SiO₃ resulted in the carbonation of salts to form carbonate, which was detrimental to the compressive strength.

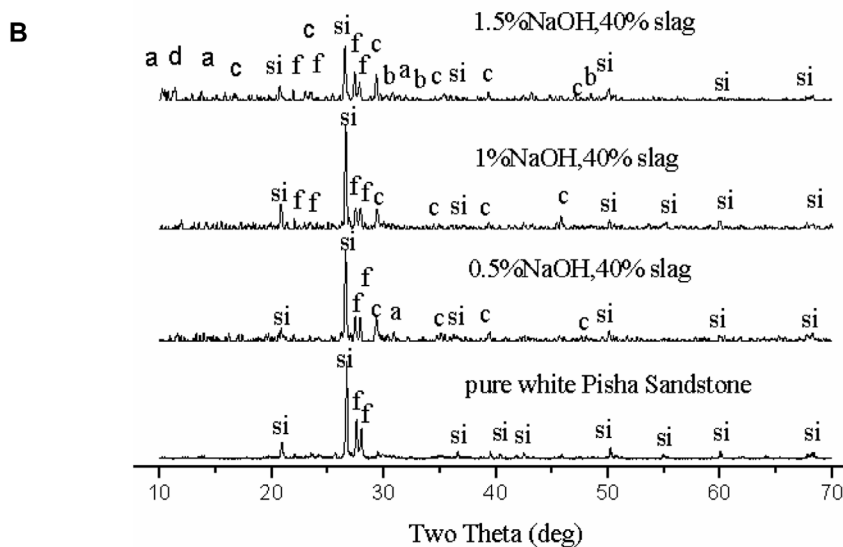
3.3 XRD analysis of the hydration products of alkali-activated white PS geopolymer cement

As shown in Figure 1, the mineral phases of white PS are quartz, faujasite, fuchsite, cronstedtite phillipsite, feldspar, ferric oxide, and pyrophyllite. XRD indicated that slag has an amorphous microstructure (Figure 1). Additionally, there were three characteristic peaks; the highest diffraction peak is at a diffraction angle of 30° (2θ). Figure 2 and Table 1 suggest that the mineral phases in the slag contain Ca₂SiO₃, Ca₃SiO₅, and active aluminium oxide. Thus, it can be added as a mineral admixture to enhance the properties of alkali-activated white PS geopolymer cement material.

The XRD patterns of samples with different slag contents and NaOH dosages were measured at 90 days. The results are shown in Figures 6A, B. Reddy and Harihanandh (2023) suggested that NaOH could possibly form Na-geopolymer gel, Ca-geopolymer gel, and C-S-H gel when reacted in geopolymer cement pastes. The Ca-geopolymer gel has better chemical



XRD patterns of specimens with different slag contents at 90 days.



XRD patterns of specimens with different NaOH dosages as an activator at 90 days.

FIGURE 6

(A) XRD patterns of specimens with different slag contents at 90 days. Notes: in (A,B): Si, quartz; f, feldspar; a, CSH gel; b, $C_{14}AH_{13}$; C= $CaCO_3$, d = C-(N)-S-H. (B). XRD patterns of specimens with different NaOH dosages as an activator at 90 days.

and physical properties than the Na-geopolymer gel. Slag with a high CaO content can improve the mechanical properties and condense the microstructure of alkali-activator white PS geopolymer cement material.

Figure 6A shows that slag has a significant effect on the characteristic peaks of alkali-activated white PS geopolymer cement at 90 days. With the increasing slag dosage, the intensity of the diffraction peaks for quartz and feldspar first increased and then descended. This was caused by the fact that the feldspar will take part in the polymerization reaction in the situation that active Si and Al are insufficient to polymerize the Al and Si network when there is a small amount of slag as a mineral additive. However, with abundant slag as a mineral additive, the active Si and Al in the pastes are sufficient to finish the polymerization reaction. Thus, a

small amount of feldspar was present in the polymerization reaction. As shown in Figure 6A, the amount of hydration products that revealed an amorphous microstructure increased with the rise of slag dosage at day 90. Two amorphous humps were observed at $2\theta \approx 10^\circ$ and 22.5° on the XRD patterns of alkali-activated white PS geopolymer cement with slag regardless of slag dosage at 90 days. However, the XRD patterns of the pure white PS showed no diffraction peaks at the same angles at 90 days. The intensity of two amorphous humps ($2\theta \approx 10^\circ$ and 22.5°) increased with the increasing slag dosage at 90 days. Extensive reviews (Snellings et al., 2022; Zhong et al., 2023) revealed that the two amorphous humps are the calcium silicate hydrate (C-S-H) gel, which can be regarded as one of the main products of hydration. However, the XRD patterns of alkali-

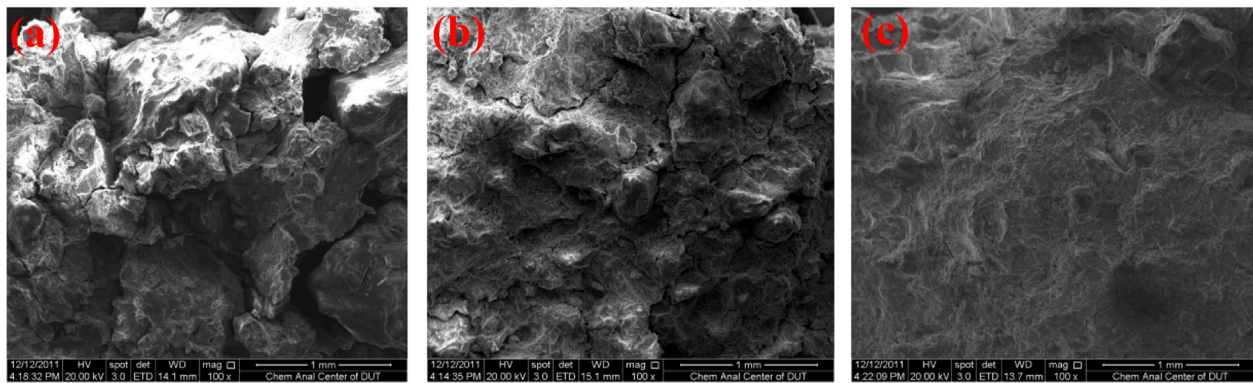


FIGURE 7
(A–C) SEM images of specimens cured for 90 days at 20°C. (A) White PS. (B) White PS with 1.5 wt.% NaOH. (C) White PS with 1.5 wt.% NaOH and 40 wt.% slag.

activated white PS geopolymer cement with slag revealed an evident steep peak consisting of calcium carbonate, which appears at $2\theta \approx 30^\circ$ at 90 days. This could be because of the carbonation of hydrated calcium silicate, calcium oxide, or calcium hydroxide in alkali-activated white PS pastes with slag at 90 days. C-(N)-S-H ($\text{Na}_2\text{Ca}_2\text{Si}_2\text{O}_7 \cdot \text{H}_2\text{O}$) gel has been observed in NaOH-activated slag (Feng and Li, 2023), which is an internal binding product formed around partially reacted slag particles. The intensity of the most prominent characteristic peak of C-(N)-S-H gels ($2\theta \approx 12^\circ$) increased with the rise in slag content and NaOH dosage at 90 days. On the other hand, $4\text{CaO} \cdot \text{Al}_2\text{O}_3 \cdot 13\text{H}_2\text{O}$ (C_4AH_{13}) is one of the minor hydration products that can gain the binder leading to higher compressive strength (Reddy and Harihanandh, 2023).

The NaOH dosage has a prominent effect on the hydration products of alkali-activated white PS when slag addition is more than 20 wt.%. The gel type of hydration products increased with the NaOH dosage, which is shown in Figure 6B. Figure 6B shows that with more NaOH as activator, the intensity of the most prominent peak of the C-S-H and C-(N)-S-H gels gradually increased. However, the dosage of the NaOH has a slight influence on the intensity of the most distinctive peak of quartz, CaCO_3 , and feldspar when there is 40 wt.% slag as a mineral additive at 90 days.

3.4 SEM/EDS analysis of the microstructures and hydration products of alkali-activated white PS geopolymer cement

3.4.1 Microstructures

Figure 7A shows that the white PS had a poor structure as there were many cracks and holes in the matrix. This is the reason that the compressive strength of white PS at 90 days is very low. However, when 1.5 wt.% NaOH and 4 wt.% Na_2SiO_3 were added as an activator, the size of the cracks and holes reduced in the matrix, as shown in Figure 7B. Additionally, the compressive strength increased by 1,088% compared with the specimens without an activator at 90 days. As demonstrated in Figure 7C, the specimens with 1.5 wt.% NaOH and 40 wt.% slag showed a dense microstructure. The cracks and holes disappeared in the matrix and the compressive strength increased by 9,011% compared with the white PS at 90 days.

3.4.2 Hydration products

Figures 8A–D shows SEM images of alkali-activated white PS geopolymer cement with 10 wt.% slag (B3), 20 wt.% slag (C3), 30 wt.% slag (D3), and 40 wt.% slag (E3) at 90 days. Table 4 shows the EDS analyses results of average values of the main elemental molar ratios for the different morphologies of hydration products. It is worth noting that the average values of the molar ratios of the major elements were determined from six different points in the hydration products of alkali-activated white PS geopolymer cement. All the samples shared the same hydration products (geopolymer, C-S-H, and CaCO_3). However, the hydration products of the samples showed quite different microstructures from each other. Table 4 shows that the molar oxide ratio of $\text{SiO}_2/\text{Al}_2\text{O}_3$ is 6.2, 5.3, 3.4, and 6.2 in the hydration products of B3, C3, D3, and E3, respectively. The studies (Gao et al., 2023; Mounika et al., 2023) suggest that the standard molar oxide ratios of $\text{SiO}_2/\text{Al}_2\text{O}_3$ in geopolymer composition are between 3.3 and 6.5 for the finished product. Thus, the geopolymer is one of the main hydration products.

Figure 8A shows a poor structure with cracks and holes caused by the hydration products that are not enough to bond and fill the matrix. Thus, the specimens of B3 showed a low compressive strength. The morphology of the hydration products obtained from Figure 8A (B3) is expected to lead to porous gel. Additionally, there was a small amount of crystal (1 μm in size), which adhered to the surface of the gel. Combined with XRD, SEM, and the calculation formula of the EDS formula analysis, hydration products can be identified as calcium carbonate crystal (3), C-S-H (1), and geopolymer (2). Figure 8B shows that the hydration products of the specimen are gel and massive crystals bonding on the surface of the gel. XRD, SEM, and EDS analysis showed that the hydration products of C3 are calcium carbonate crystals (3), $3\text{CaO} \cdot \text{SiO}_2 \cdot 8\text{H}_2\text{O}$ (1), and geopolymer (2). The morphologies of the hydration products obtained from D3 and E3 revealed massive geopolymer gels (2), C-S-H and C-(Na)-S-H gel (1), and a few sodium carbonates, which made the matrix form a dense structure. Therefore, the samples of D3 and E3 showed a higher compressive strength than those of B3 and C3. There were many nanosized calcium carbonate crystals (3) adhering to the surface of the gel in Figure 8C. However, Figure 8D shows a few calcium carbonate crystals (3) of 0.3 μm in size and massive nanosized C-S-H (1) in the

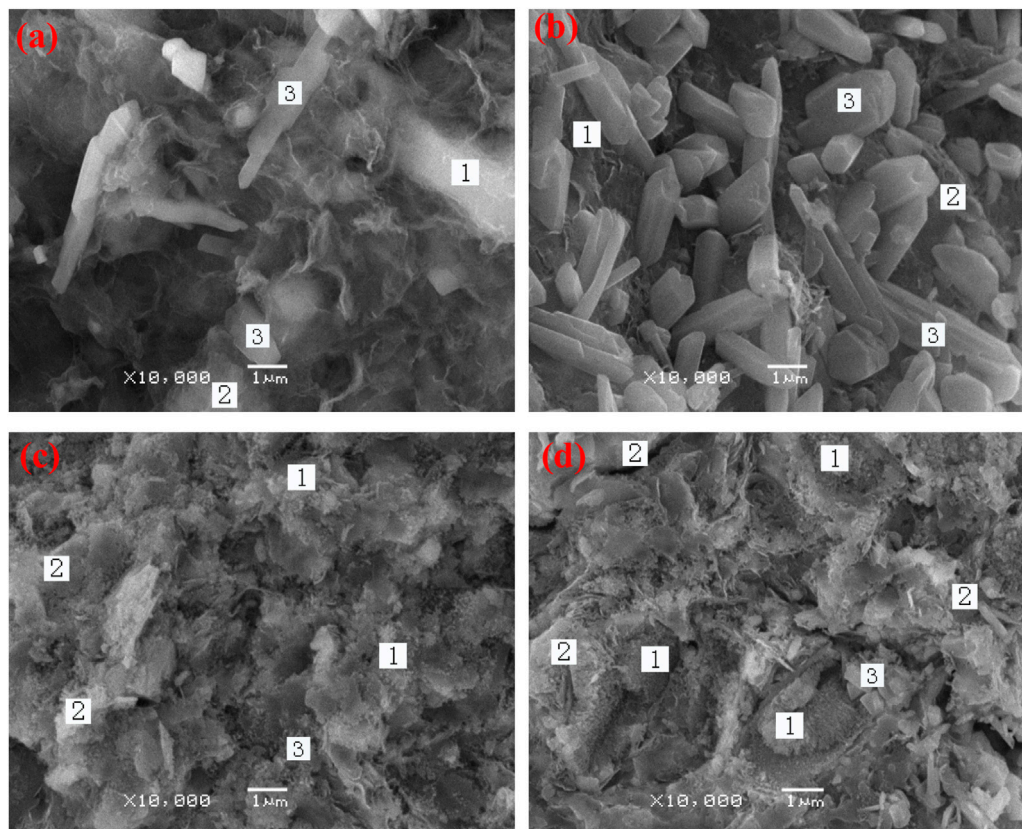


FIGURE 8
(A–D) SEM images of alkali-activated white PS with 10 wt.% slag (B3), 20 wt.% slag (C3), 30 wt.% slag (D3), and 40 wt.% slag (E3) at 90 days.

TABLE 4 The average values of the main elemental molar ratios in alkali-activated white PS at 90 days observed in EDS.

| Specimens | C | O | Na | Mg | Al | Si | K | Ca |
|-----------|------|------|-----|-----|-----|------|-----|------|
| B3 | 15.1 | 60.1 | 2.7 | 3.3 | 3.2 | 10.1 | 0.1 | 5.1 |
| C3 | 8.5 | 61.1 | 1.1 | 0.9 | 1.7 | 4.5 | 2 | 20.3 |
| D3 | 5.3 | 61.1 | 1.6 | 5.9 | 5.3 | 9.2 | 0.1 | 9.1 |
| E3 | 10.1 | 65.3 | 3.3 | 1.5 | 5.1 | 12.8 | 0.1 | 1.4 |

pores of the matrix. The formation of a large amount of nanosized C-S-H in E3 resulted in the highest compressive strength.

3.5 TG/DTG analysis of the hydration products of alkali-activated white PS geopolymer cement

The effect of slag content on hydration products is shown in Figure 9, which demonstrates that the weight loss of samples were divided into three regions: 50°C–100°C [free water (W) loss regions], 100°C–500°C (the water loss regions of the hydration products), and 500°C–800°C (the CO₂ loss regions of CaCO₃) (Mounika et al., 2023). In particular, 100°C–500°C, which was shown by the DTG data of PS, is the water

loss region of clastic organics. Additionally, the DTG data also showed that there is a small amount of calcium carbonate, which had lower crystallinity in PS. The DTG data shows that the speed of weight loss for C3 was faster than B3 in the 100°C–500°C region, indicating that C3 had more hydration products at 90 days. The water losses (100°C–500°C) of PS, B3, and C3 were 3.52%, 3.66%, and 4.17%, respectively. However, at the regions of CO₂ loss, B3 showed a faster trend of weight loss than C3. This meant that B3 had a higher carbonation content than C3. The amount of CO₂ loss of CaCO₃ increased from 4.54 wt.% to 5.01 wt.% with the increase in slag addition. However, the carbonation ratios of B3 and C3 were 49.3% $\{[(56/44) \times 4.53\%] / 11.7\}$ and 41.3% $\{[(56/44) \times 5.04\%] / 15.53\}$ at 90 days, respectively. Thus, high slag addition decreased the carbonation ratio of C-S-H gel.

The results of XRD, SEM and EDS showed that the growth in strength of alkali-activated white PS geopolymer cement can be considered to be the result of the contribution of geopolymer gel and C-S-H gel. This is similar to the result of Sha (Sha et al., 2021; Han et al., 2023; Li et al., 2023; Mohammed and Yaltay, 2023; Shen et al., 2023; Wu et al., 2023). This study suggested that the strength of geopolymer cement containing active mineral additive can be divided into two parts. The main contributor to strength for this type of cement is the polymerized Al and Si network obtained from the reaction between active Si and Al in the pastes. The secondary part of contribution of the strength is formation of semi-crystalline tobermorites or calcium aluminosilicate hydrates. However, the present study showed that the addition of more slag

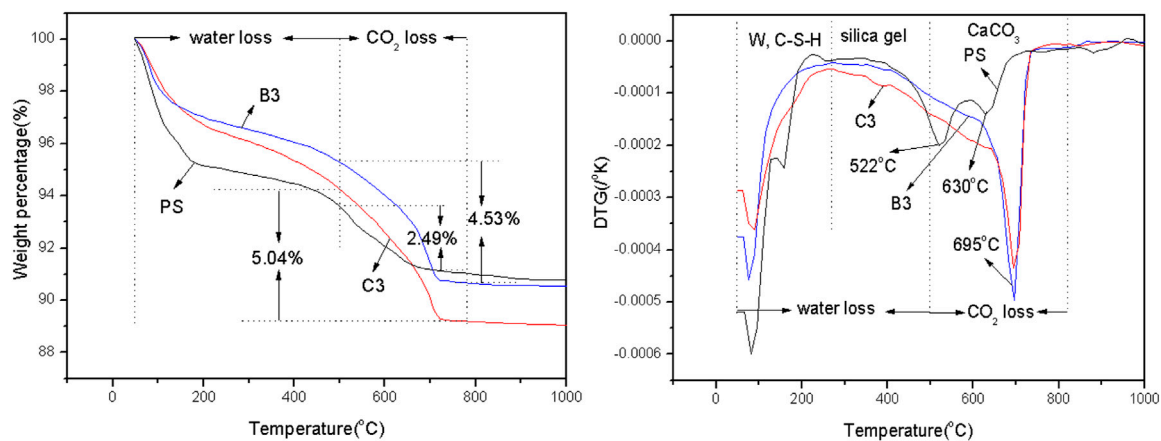


FIGURE 9
Thermogravimetric analysis of white PS, B3, and C3 at 90 days.

and NaOH led to less formation of calcium carbonate resulting from the carbon dioxide of the atmosphere and C-S-H in alkali-activated white PS geopolymer cement.

4 Conclusion

This study succeeded in converting PS into geopolymer cement, which has better mechanical properties and denser microstructure performance. The mechanical properties, the reaction mechanism, and hydration products of alkali-activated PS were investigated. The following conclusions could be drawn:

- (1) The white PS showed better potential than red PS as a source of aluminosilicate for use in geopolymer cement production. The compressive strength of pure white and red PS with activator increased by 1,088% and 692% compared with the compressive strength of pure white and red PS without activator.
- (2) The insufficiency of active SiO_2 , active Al_2O_3 , and active CaO in white PS can be compensated by adding slag. The compressive strength greatly increased with the increase in slag dosage. The compressive strength of alkali-activated white PS geopolymer cement with 40 wt.% slag and 1.5 wt.% NaOH reached 82 MPa at 90 days, which increased by 9,011% compared with that of alkali-activated white PS geopolymer cement without slag.
- (3) The NaOH dosage has a significant effect on the compressive strength of alkali-activated PS geopolymer cement. The compressive strength of alkali-activated PS geopolymer cement significantly increased with the increasing NaOH dosage from 0.5 wt.% to 1.5 wt.%. At 90 days, the compressive strength of the samples with 40 wt.% slag increased from 63 to 82 MPa (a 30.2% increase) as the NaOH dosage increased from 0.5 wt.% to 1.5 wt.%.
- (4) The main hydration products of alkali-activated PS geopolymer cement are C-S-H gel, geopolymer gel, and calcium carbonate crystals. The formation of calcium carbonate crystals was caused by the reaction between $\text{Ca}(\text{OH})_2$ or C-S-H gel and carbon dioxide from atmosphere. There was a serious carbonation of C-S-H gel in alkali-activated PS geopolymer cement. The TG/DTG data showed

that there was a lower carbonation ratio of C-S-H gel and more hydration products when adding more slag. When 10% slag and 1.5% NaOH as an activator was used, the carbonation ratio of C-S-H gels in alkali-activated PS geopolymer cement decreased from 49.3% to 41.3% as the slag content increased from 10 wt% to 20 wt.%.

Data availability statement

The original contributions presented in the study are included in the article/Supplementary Material, further inquiries can be directed to the corresponding author.

Author contributions

JD: Methodology, Resources, Writing—original draft. LL: Methodology, Validation, Writing—original draft. ZS: Data curation, Formal Analysis, Writing—original draft. YD: Data curation, Writing—original draft, Writing—review and editing. XC: Conceptualization, Visualization, Writing—original draft. YZ: Data curation, Formal Analysis, Writing—original draft.

Funding

The author(s) declare financial support was received for the research, authorship, and/or publication of this article. This research was funded by the National Natural Science Foundation of China (52163034) and the Natural Science Foundation of Jiangxi Province, China (20232BCJ23029).

Conflict of interest

The authors declare that the research was conducted in the absence of any commercial or financial relationships that could be construed as a potential conflict of interest.

Publisher's note

All claims expressed in this article are solely those of the authors and do not necessarily represent those of their affiliated

organizations, or those of the publisher, the editors and the reviewers. Any product that may be evaluated in this article, or claim that may be made by its manufacturer, is not guaranteed or endorsed by the publisher.

References

- Abdellatif, M., Elrahman, M. A., Alanazi, H., Abadel, A. A., and Tahwia, A. (2023). A state-of-the-art review on geopolymer foam concrete with solid waste materials: components, characteristics, and microstructure. *Innov. Infrastruct. Solutions* 8 (9), 230. doi:10.1007/s41062-023-01202-w
- Alaneme, G. U., Olonade, K. A., and Esenogho, E. (2023). Critical review on the application of artificial intelligence techniques in the production of geopolymer-concrete. *SN Appl. Sci.* 5 (8), 217. doi:10.1007/s42452-023-05447-z
- Dhakal, M., Scott, A. N., Dhakal, R. P., and Clucas, D. (2022). Structural and durability properties for magnesia alumina silicate concrete. *Constr. Build. Mater.* 340, 127725. doi:10.1016/j.conbuildmat.2022.127725
- Feng, B., and Liu, J. (2022). Durability of repair metakaolin geopolymeric cement under different factors. *Processes* 10 (9), 1818. doi:10.3390/pr10091818
- Feng, Z., and Li, X. (2023). Microbially induced calcite precipitation and synergistic mineralization cementation mechanism of Pisha sandstone components. *Sci. Total Environ.* 866, 161348. doi:10.1016/j.scitotenv.2022.161348
- Fu, H., Guo, X., Zhou, P., Yan, P., Zheng, Y., Liu, L., et al. (2021). Modification of low-density slag cementing slurry with SiC whiskers at high temperature. *Adv. Mater. Sci. Eng.* 2021, 1–9. doi:10.1155/2021/9586645
- Gao, N., Xiao, Q., and Zhang, P. (2021). Characteristics of eroded sediment particles on Pisha sandstone slopes under compound erosion. *J. Soil Water Conservation* 35 (1), 44–49. doi:10.13870/j.cnki.stbcbx.2021.01.006
- Gao, Y., Zhu, Z., Meng, H., Hu, X., and Li, Z. (2023). Synergistic enhancement mechanism of calcium carbide Residue/Desulfurization gypsum -steel slag modified fly ash geopolymer. *J. Build. Mater.* 26 (08), 870–878. doi:10.3969/j.issn.1007-9629.2023.08.007
- Han, X., Zhang, P., Zheng, Y., and Wang, J. (2023). Utilization of municipal solid waste incineration fly ash with coal fly ash/metakaolin for geopolymer composites preparation. *Constr. Build. Mater.* 403, 133060. doi:10.1016/j.conbuildmat.2023.133060
- Li, Y., Shen, J., Lin, H., and Li, Y. (2023). Optimization design for alkali-activated slag-fly ash geopolymer concrete based on artificial intelligence considering compressive strength, cost, and carbon emission. *J. Build. Eng.* 75, 106929. doi:10.1016/j.jobeb.2023.106929
- Liu, M., Yang, D., Chen, L., Chen, G., and Ma, Z. (2023b). Effect of silicate modulus and alkali content on the microstructure and macroscopic properties of alkali-activated recycled powder mortar. *Constr. Build. Mater.* 397, 132365. doi:10.1016/j.conbuildmat.2023.132365
- Liu, W., Huang, Z., Guo, Z., López-Vicente, M., Wang, Z., and Wang, Z. (2023a). A nature-based solution to reduce soil water vertical leakage in arid sandy land. *Geoderma* 438, 116630. doi:10.1016/j.geoderma.2023.116630
- Luo, X., Li, S., Guo, Z., Liu, C., and Gao, J. (2022). Effect of curing temperature on the hydration property and microstructure of Portland cement blended with recycled brick powder. *J. Build. Eng.* 61, 105327. doi:10.1016/j.jobeb.2022.105327
- Luo, Y., Zhang, Q., Wang, D., Yang, L., Gao, X., Liu, Y., et al. (2023). Effect of sodium methyl-silicate on the performance and structure of geopolymer. *Mater. Lett.* 350, 134893. doi:10.1016/j.matlet.2023.134893
- Lv, Y., Wang, S., Ge, Y., Xiao, B., and Peng, H. (2021). Influence of slag content on alkalinity of pore solution and polymerization behavior of metakaolin-based geopolymer. *J. Central South Univ. Technol.* 52 (12), 4434–4442. doi:10.11817/j.issn.1672-7207.2021.12.023
- Mohammed, D. T., and Yaltay, N. (2023). Strength and elevated temperature resistance properties of the geopolymer paste produced with ground granulated blast furnace slag and pumice powder. *Ain Shams Eng. J.* 2023, 102483. doi:10.1016/j.asej.2023.102483
- Mounika, G., Ramakrishna, U., Reddy, K., and Kumar, S. (2023). A review on effect of red mud on properties of alkali activated materials (AAMs) and geopolymers (GPs). *Mater. Today Proc.* doi:10.1016/j.matpr.2023.03.446
- Pratap, B., Mondal, S., and Rao, B. H. (2023). NaOH molarity influence on mechanical and durability properties of geopolymer concrete made with fly ash and phosphogypsum. *Structures* 56, 105035. doi:10.1016/j.istruc.2023.105035
- Reddy, Y., and Harihanandh, M. (2023). Experimental studies on strength and durability of alkali activated slag and coal bottom ash based geopolymer concrete. *Mater. Today Proc.* doi:10.1016/j.matpr.2023.03.644
- Sha, D., Pan, B., Li, Y., and Wang, B. (2021). Study on preparation and performance of alkali-activated coal-based synthetic natural gas slag geopolymer. *China J. Highw. Transp.* 34 (10), 234–244. doi:10.19721/j.cnki.1001-7372.2021.10.019
- Shen, Y., Kang, S., Cheng, G., Wang, J., Wu, W., Wang, X., et al. (2023). Effects of silicate modulus and alkali dosage on the performance of one-part electric furnace nickel slag-based geopolymer repair materials. *Case Stud. Constr. Mater.* 19, e02224. doi:10.1016/j.cscm.2023.e02224
- Snellings, R., Machner, A., Bolte, G., Kamyab, H., Durdzinski, P., Teck, P., et al. (2022). Hydration kinetics of ternary slag-limestone cements: impact of water to binder ratio and curing temperature. *Cem. Concr. Res.* 151, 106647. doi:10.1016/j.cemconres.2021.106647
- Wang, Y., Li, C., Ge, X., and Gao, L. (2022). Experimental study on improvement of weathered Pisha sandstone soil in Inner Mongolia section of the Yellow River Basin based on microbially induced carbonate precipitation technology. *Rock Soil Mech.* 43 (03), 708–718. doi:10.16285/j.rsm.2021.1010
- Wei, W. Y., Xiao, P. Q., and Zhang, P. (2020). Experiment on runoff and sediment production process of Pisha sandstone slope under composite erosion. *J. Soil Water Conservation* 34 (2), 18–22. doi:10.13870/j.cnki.stbcbx.2020.02.003
- Wu, H., Liang, C., Yang, D., and Ma, Z. (2023). Development of sustainable geopolymer materials made with ground geopolymer waste powder as renewable binder up to 100%. *Constr. Build. Mater.* 400, 132746. doi:10.1016/j.conbuildmat.2023.132746
- Wu, J., Guo, L., Cao, Y., and Qin, Y. (2022). Effect of steam curing system on the early mechanical property and microstructure of ultra-high performance concrete. *J. Southeast Univ. Sci. Ed.* 52 (04), 744–752. doi:10.3969/j.issn.1001-0505.2022.04.016
- Wu, J., Zheng, X., Yang, A., and Li, Y. (2021). Experimental study on the compressive strength of muddy clay solidified by the one-part slag-fly ash based geopolymer. *Rock Soil Mech.* 42 (03), 647–655. doi:10.16285/j.rsm.2020.0918
- Yang, D., Lu, M., Song, D., Bai, S., Zhang, G., Hu, X., et al. (2021). Research progress of geopolymer cement. *Mater. Rep.* 35 (S1), 644–649.
- Yi, P. L., Qian, Z., Defa, W., Yang, L., Gao, X., Liu, Y., et al. (2023). Mechanical and microstructural properties of MK-FA-GGBFS-based self-compacting geopolymer concrete composites. *J. Build. Eng.* 77, 107452. doi:10.1016/j.jobeb.2023.107452
- Zhang, P., Yao, W., Xiao, P., Liu, G., and Yang, C. (2022). Interactive superposition effect of multi-dynamic erosion in the Pisha sandstone area of the Yellow River basin. *J. Hydraulic Eng.* 53 (01), 109–116. doi:10.13243/j.cnki.slxb.20210349
- Zhong, Q., Nie, H., Xie, G., and Peng, H. (2023). Experimental study on the characteristics, rheological factors, and flowability of MK-GGBFS geopolymer slurry. *J. Build. Eng.* 76, 107300. doi:10.1016/j.jobeb.2023.107300